Quantifying Thermophoretic Deposition of Soot on Surfaces

Amy Mensch, Thomas Cleary
National Institute of Standards and Technology, Gaithersburg, MD, USA

Abstract

Quantitative data on deposition of soot agglomerate particles in the literature is needed to advance fire forensic analysis as well as fire model predictions of visibility and detector activation. This paper provides direct measurements of thermophoretic soot deposition in a laminar flow channel and the driving conditions to improve understanding of soot deposition in fires and for deposition model assessment. The overall deposition velocities were determined through measurements of the incoming soot concentration and gravimetric measurements of the soot deposited. The effects of channel flowrate and temperature gradient as well as inlet concentration were examined. The deposition velocities showed good agreement with the theoretical thermophoretic velocities based on the channel temperature gradients. The flow, heat transfer and deposition were also modeled using the Fire Dynamics Simulator, and the simulation deposition velocities were generally less than those found in the experiments.

Keywords: soot, thermophoresis, deposition velocity

Introduction

The physics of soot deposition in fires are controlled by thermophoretic, turbulent and gravitational deposition mechanisms. The thermophoretic mechanism is driven by temperature gradients in the gas, which impart unequal collision energies on aerosol particles between the hot and cold sides, resulting in motion in the opposite direction of the temperature gradient. The focus of this study is on thermophoretic deposition, which has a significant role in fires, especially for small particles (0.1 μm to 1 μm) [1] produced during flaming combustion.

Thermophoretic deposition is characterized by the terminal velocity of particles driven by thermophoresis. The theoretical thermophoretic velocity, v_{th}, is proportional to the temperature gradient, ∇T, and the

kinematic viscosity, ν, of the gas, and inversely related to the temperature of the particle, T_p:

$$v_{th} = -K_{th} \frac{\nu \nabla T}{T_p} \quad \text{(Eq. 1)}$$

K_{th} is the thermophoretic coefficient. For a Knudsen number (the ratio of gas mean free path to particle radius), Kn >> 1, when the mean free path of the gas is much greater than the particle size, K_{th} is generally assumed to be 0.55 and independent of particle size [2]. This condition is known as the free molecular regime. K_{th} can also be calculated as a function of Kn (which is a function of particle size and gas temperature), the thermal conductivities of the gas and particle, and empirical constants [3]. Studies of soot agglomerates have generally found that K_{th} should be evaluated using the primary particle diameter [4]–[6], suggesting the use of K_{th} = 0.55 for soot. Suzuki et al. [6] noted that K_{th} also depends on the morphological characteristics of the agglomerates, with more open structures being closer to the free molecular regime compared with more compact agglomerates.

Currently, there is insufficient validation data to assess the performance of predictive models of thermophoretic soot deposition. Researchers have used different approaches to measure soot deposition from fires, including optical scanning of glass paper deposition targets [7], directly measuring physical thickness [8], and measuring the response of a conductometric gauge [9]. Several soot deposition studies [4], [10], [11], motivated by the need to monitor soot in diesel exhaust, generated either indirect or qualitative measurements of surface deposition.

Soot deposition experiments

The mechanism behind thermophoretic deposition was studied within a thin rectangular laminar flow channel with a transverse temperature gradient applied across the channel height, ensuring that deposition occurred only on the cold side of the channel. The channel was positioned so the flow was vertically downward to remove the effect of gravitational deposition. The flow passed through a plenum before and after the flow channel to minimize entrance and exit effects. The side walls were polytetrafluoroethylene, and the cold and hot boundaries were aluminum slabs, 19.1 mm thick to approximate constant temperature boundaries. On the outer side of the cold wall was a serpentine copper line circulating cold water, resulting in outer cold wall temperatures between 15 °C and 20 °C. On the outer side of the hot wall was a resistance heater with on-off control based on a set point temperature measured on the outer side of the hot wall. This temperature was set to 230 °C and 120 °C to generate cases with internal temperature differences of approximately 200 °C and 100 °C.

A steady-state flow simulation, which included the inlet plenum geometries, predicted fully-developed flow and temperature profiles by

20 % of the channel length for a channel flow of 3 SLM (standard L/min) and 50% of the channel length for 10 SLM [12]. The flow was laminar for both flowrates, using the Reynolds number based on the hydraulic diameter of the channel (< 230 for all cases). The fully-developed temperature profiles were confirmed to be linear across the channel height. The channel geometry is depicted in Fig. 1.

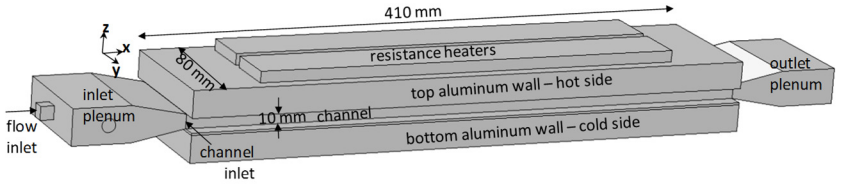

Fig. 1 Diagram of experimental channel geometry.

A laminar diffusion flame burner was used to generate soot for deposition. Propene fuel exited a 10 mm diameter tube surrounded by co-flow air from a 120 mm diameter ceramic honeycomb, enclosed by a brass chimney. After a tripper plate to induce mixing, additional dilution air was injected into the upper stage of the burner. All fuel and air flows to the burner, 0.055 SLM and 0.077 SLM for the fuel, 54.08 SLM for the co-flow air, and 32.47 SLM for the dilution air, were set by mass flow controllers. The duration of deposition exposures ranged from 15 min to 60 min. The soot aerosol concentration, C_p, entering the channel was measured by two methods, by flowing part of the exhaust from the burner through a tapered element oscillating microbalance (TEOM), and by flowing part of the exhaust through a filter to measure the change in mass captured at the measured flowrate. The averages and expanded uncertainties at 95 % confidence interval (μ) of C_p are given in Table 1.

Table 1. Particle concentration, C_p, measurements.

Fuel flow (L/min)	$C_{p,ave}$ (mg/m^3)		No. of experiments	μ of $C_{p,ave}$ (mg/m^3)	μ of C_p, in each experiment
0.055	TEOM	**66**	21	± 21.0	± 6.1
	Filter	**70**	15	± 5.4	± 7.5
0.077	TEOM	**108**	3	± 10.4	± 39.0
	Filter	**125**	11	± 19.2	± 11.4

At the end of the exposure the mass loading of soot deposited on the cold side of the channel was determined gravimetrically by measuring the change in mass, m_{dep}, on four aluminum foil circular targets (each with A_{dep} = 1.7E-03 m^2). The targets were spaced along the channel centerline, centered at 30 mm, 132 mm, 233 mm, and 335 mm from the channel inlet. The mass of the targets was taken at least several hours

after the end of an experiment, after the channel was cooled to room temperature. Subsequent mass measurements performed after desiccating overnight did not show consistent reductions to indicate condensed volatiles or water on the targets. The uncertainty in mass loading measurements was estimated as ± 1 mg/m^2. The standard deviation over the average of the four mass loading measurements was 15 % or less for all but one experiment, with the biggest deviation coming from the first target. The average mass loading, the incoming C_p, and the exposure time, t, were used in Eq. 2 to calculate the overall deposition velocity, v_{dep}. The filter-based C_p was used for experiments when the filter was included. Otherwise, the TEOM-based C_p was used.

$$v_{dep} = \frac{m_{dep}}{C_p A_{dep} t} \qquad \text{(Eq. 2)}$$

The average v_{dep} from each experiment could be compared to the theoretical v_{th} determined from Eq. 1 because the thermophoretic force was the major mechanism driving particles to deposit, and the flow and C_p were steady throughout the experiments. Because of the linear temperature gradient across the channel, the ∇T for the calculation of v_{th} was determined based on surface temperature measurements from steady-state experiments without deposition [12]. The average of the temperatures measured at the inlet and outlet was used to estimate T_p. Table 2 reports ∇T and T_p for the different cases of flow and ΔT. A K_{th} of 0.36 was used to achieve the best matching of v_{th} with v_{dep}.

Table 2. Channel flow and thermal measurements.

	ΔT = 200 °C		ΔT = 100 °C	
Channel flow (SLM)	3.00	10.00	3.00	10.00
Measured ∇T (°C/m)	19745	19704	10394	10408
Measured T_p (°C)	69	77	47	57

The results comparing the measured v_{dep} and the calculated v_{th} are plotted in Fig. 3 with the dashed line representing correspondence between the two velocities. Each symbol represents one experiment, with different color symbols representing different fuel flows or measurement methods for C_p. The error bars show the estimated combined expanded uncertainties, which were ±15 % for v_{th} and varied from ±7.5 % to ±11.3 % for v_{dep}. The primary factor that affected deposition velocity was the applied temperature gradient of the exposure. The cases with ΔT of 200 °C are clustered between 0.4 mm/s and 0.5 mm/s, and the cases with ΔT of 100 °C are clustered around 0.2 mm/s. One data point had error bars outside of the dotted line (v_{dep} = 0.14 mm/s, v_{th} = 0.21 mm/s). This point was for a channel flow of 10 L/min and ΔT of 100 °C. For this case the mass deposited on the first target was significantly lower than the average of the four targets, and its standard deviation over the average was 24 %. The local

temperature gradient close to the cold surface could be lower than expected before the thermal profile was fully-developed, and therefore have locally reduced deposition. Indirectly, the channel flow could affect deposition velocity through changes to the flow and temperature profiles. However, the cases with 10 SLM and ΔT of 200 °C did not have significantly less deposition on the first target, and the overall average deposition velocities were close to the dotted line in Fig. 3. The C_p and fuel flow also could have indirectly affected deposition velocity through changes to the soot size distribution, but there was no apparent distinction in cases with different fuel flowrates. Therefore, it was found that temperature gradient, and not C_p, fuel flow, or channel flow, directly affected deposition velocity, as expected based on Eq. 1.

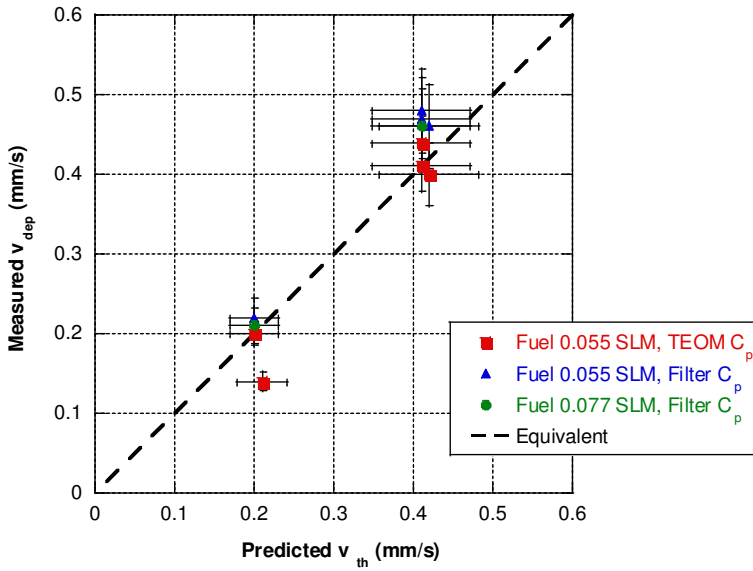

Fig. 3. Experimental v_{dep} versus predicted v_{th}.

Computational modelling

To model the soot deposition within the channel, computational flow and heat transfer simulations were run using the NIST Fire Dynamics Simulator (FDS) [3], [13]. The simulations were transient to track the buildup of soot on the surface. In FDS's aerosol deposition models, soot was treated as an additional gaseous species for which diffusive transport along concentration gradients was calculated automatically. To account for thermophoretic transport, an additional velocity based on Eq. 1 was applied to the aerosol species. Soot was introduced into the inlet flow at a concentration of 70 mg/m^3, although this value did not affect v_{th} or the distribution of soot deposition, only the amount of deposit. The default soot properties from FDS were used, except for particle diameter, which was specified to be 0.035 µm, as an estimate

of the primary particle size of soot agglomerates [6]. FDS used the temperature in the first grid cell above the wall for T_p and the temperature dependent properties needed to calculate v_{th}. The K_{th} was calculated to be 0.55 in the FDS simulations.

The computational mesh was a structured rectangular grid with spacing of 5 mm across the width and length, and 1 mm across the height. The simulations were run for 1000 s, with steady deposition rates reached by 10 s. The hot and cold wall boundary conditions were constant temperature, and the side walls were adiabatic to approximate the experimental conditions. The inlet flow profile was prescribed based on the steady-state flow solution that included the inlet plenum geometry, while the flow temperature for the inlet was determined from the measurements within the inlet plenum.

Fig. 4 shows the FDS results for deposition velocity, v_{FDS}, just above the cold wall. The value of v_{FDS} covering the largest area in the downstream portion of the channel is labeled for each case. When ΔT was doubled from 100 °C to 200 °C, the v_{FDS} results were slightly more than doubled. When the channel flow increased from 3 SLM to 10 SLM, v_{FDS} decreased slightly for both temperature differences. The v_{FDS} increased along the flow direction as the flow and temperature profiles developed. The increases in v_{FDS} continued farther into the channel for the 10 SLM cases compared to the 3 SLM cases, which were more stable in the downstream half of the channel. These differences between the channel flowrates were attributed to the differences in the flow development, with 10 SLM requiring a longer channel distance to completely develop. In general, v_{FDS} predictions were lower than v_{dep} and v_{th} from corresponding experiments, except for the downstream v_{FDS} for the 3 SLM cases, which were close to the v_{dep} and v_{th}.

Two significant aspects of the FDS thermal predictions are affecting the deposition velocity comparisons with the experiments. First, the development length for fully-developed temperature profiles in FDS is longer than expected in the experiments based on the detailed steady-state flow simulations [12]. Fully-developed profiles in the experiments are also confirmed by the uniformity of soot loading measurements across the length, particularly for the final three out of four targets. The second discrepancy is with the values calculated for ∇T in FDS, which are significantly less than the measured ∇T's in Table 2. FDS determines ∇T using wall heat transfer coefficient correlations [3], which may be causing errors to v_{FDS} for these cases of laminar channel flow.

Conclusion

Laminar flow through a thin rectangular channel with a transverse temperature gradient was used to generate thermophoretic deposition exposures on a target surface for different cases of channel flowrate, channel temperature gradient, and fuel flowrate. The mass of deposition

was measured gravimetrically and combined with measurements of the inlet soot concentration to determine the overall deposition velocity. The deposition velocity compared well with the predicted thermophoretic velocities based on the channel temperature gradient and an assumed particle diameter. The channel flow was also modeled with FDS to generate predictions of soot deposition in the channel. The simulated deposition velocities showed the expected trends with temperature gradient, but were generally lower than the experimental deposition and thermophoretic velocities. The differences in the deposition velocities and thermophoretic coefficients were attributed to FDS predicting slower thermal development compared to the experiments, and to FDS calculating the temperature gradient from the heat transfer coefficient, rather than from the overall channel temperature difference.

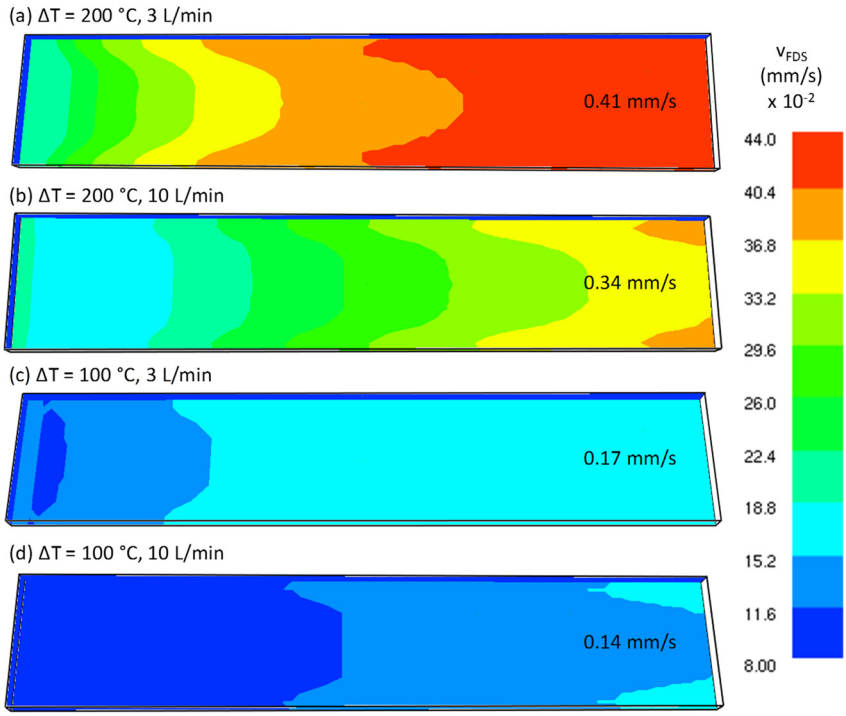

Fig. 4. FDS results for deposition velocity distribution.

References

[1] K. M. Butler and G. W. Mulholland, "*Generation and Transport of Smoke Components*," *Fire Tech.*, vol. 40, no. 2, pp. 149–176, Apr. 2004.

[2] W. C. Hinds, *Aerosol technology: properties, behavior, and measurement of airborne particles*, 2nd ed. New York: Wiley, 1999.

[3] K. McGrattan, S. Hostikka, R. McDermott, J. Floyd, C. Weinschenk, and K. Overholt, "*Fire Dynamics Simulator Technical Reference Guide Volume 1: Mathematical Model*," NIST Special Publication 1018–1, Apr. 2015.

[4] A. Messerer, R. Niessner, and U. Pöschl, "*Thermophoretic deposition of soot aerosol particles under experimental conditions relevant for modern diesel engine exhaust gas systems*," *J. of Aerosol Science*, vol. 34, no. 8, pp. 1009–1021, Aug. 2003.

[5] D. E. Rosner and Y. F. Khalil, "*Particle Morphology- and Knudsen Transition-Effects on Thermophoretically Dominated Total Mass Deposition Rates From 'Coagulation-Aged' Aerosol Population*," *J. of Aerosol Science*, vol. 31, no. 3, pp. 273–292, Mar. 2000.

[6] S. Suzuki, K. Kuwana, and R. Dobashi, "*Effect of particle morphology on thermophoretic velocity of aggregated soot particles*," *Int. J. of Heat and Mass Transfer*, vol. 52, no. 21–22, pp. 4695–4700, Oct. 2009.

[7] S. Riahi and C. Beyler, "Measurement and Prediction of Smoke Deposition from a Fire Against a Wall," *Fire Safety Science*, vol. 10, pp. 641–654, 2011.

[8] W. D. Ciro, E. G. Eddings, and A. F. Sarofim, "*Experimental and Numerical Investigation of Transient Soot Buildup on a Cylindrical Container Immersed in a Jet Fuel Pool Fire*," *Comb. Sci. and Tech.*, vol. 178, no. 12, pp. 2199–2218, Jun. 2006.

[9] T. Cleary, "*Effects of Soot Deposition on Current Leakage in Electronic Circuitry*," in *Proc. of the 15th Int. Conf. on Automatic Fire Detection (AUBE)*, 2014.

[10] G. Hagen, C. Feistkorn, S. Wiegärtner, A. Heinrich, D. Brüggemann, and R. Moos, "*Conductometric Soot Sensor for Automotive Exhausts: Initial Studies*," *Sensors*, vol. 10, no. 3, pp. 1589–1598, Mar. 2010.

[11] D. Lutic *et al.*, "*Detection of Soot Using a Resistivity Sensor Device Employing Thermophoretic Particle Deposition*," *J. of Sensors*, vol. 2010, p. 421072, Jun. 2010.

[12] A. Mensch and T. Cleary, "*EL Exploratory Project: A Soot Deposition Gauge for Fire Measurements*," National Institute of Standards and Technology, NIST TN, In progress.

[13] K. McGrattan, R. McDermott, C. Weinschenk, K. Overholt, S. Hostikka, and J. Floyd, "F*ire Dynamics Simulator User's Guide 6th Edition*," NIST Special Publication 1019, Apr. 2015.